# Characterization of new Sb2O3-based multicomponent heavy metal oxide glasses

Ali Erçin Ersundu, Miray Çelikbilek, Mohamed Baazouzi, Mohamed Toufik Soltani, Johann Troles, Süheyla Aydin

# Characterization of new $Sb_2O_3$-based multicomponent heavy metal oxide glasses

**A.E. Ersundu[1*], M. Çelikbilek[2], M. Baazouzi[3], M. T. Soltani[3], J. Troles[4], S. Aydin[2]**

[1]Nişantaşı University, Department of Mechanical Engineering, Istanbul, Turkey
[2]Istanbul Technical University, Department of Metallurgical and Materials Engineering, Istanbul, 34469, Turkey
[3]University of Biskra, Laboratory of Physics of Photonics and Multifunctional Nanomaterials, BP 145, RP, 07000, Biskra, Algeria
[4] Equipe Verres et Céramiques, UMR-CNRS 6226, Sciences Chimiques de Rennes, Université de Rennes I, 35042 Rennes Cedex, France

[*]Corresponding author
A.E. Ersundu

Nişantaşı University,
Department of Mechanical Engineering,
Istanbul, Turkey

E-mail address: ersundu@gmail.com
phone: +90 212 210 10 10
fax: +90 212 224 00 90

**Abstract**

New $Sb_2O_3$-based multicomponent heavy metal oxide glasses in the $Sb_2O_3$-$Na_2O$-$WO_3$-PbO system were prepared using a conventional melt-quenching technique. Glass formation behavior of these glasses and their thermal, physical and structural properties were investigated using X-ray diffraction (XRD), scanning electron microscopy and energy dispersive X-ray spectroscopy (SEM/EDS), differential scanning calorimetry (DSC), UV-Vis-NIR spectroscopy and Fourier transform infrared (FTIR) spectroscopy analyses according to the increasing PbO concentration by keeping the $Sb_2O_3/WO_3$ ratio constant. Thermal analysis of the glasses were realized in terms of glass transition temperature ($T_g$), crystallization temperature ($T_c/T_p$), glass stability against crystallization ($\Delta T$), activation energy of the glass transition reaction ($E_g$) and fragility parameter ($m$). Density ($\rho$), molar volume ($V_M$), oxygen molar volume ($V_O$), oxygen packing density (OPD), refractive index, band gap energy ($E_g$), average cross-link density ($\overline{n_c}$), number of bonds per unit volume ($n_b$) and Poisson's ratio ($\mu_{cal}$) values were calculated for the interpretation of physical and structural properties of the glasses. FTIR spectra of the glasses were evaluated in terms of structural transformations on the glass network.

**Keywords:** Antimony oxide, Heavy metal oxide glasses, Thermal behavior, FTIR spectroscopy

## 1. Introduction

Until today, conventional glass formers such as $SiO_2$, $B_2O_3$, $GeO_2$ or $P_2O_5$ have been preferred in opto-electronic applications. However, due to their limited infrared transmission, high optical losses and low solubility of rare-earth ions in glass network, considerable attention has been focused on the investigation of new glass types which demonstrate better optical properties. In this respect, heavy metal oxide glasses have attracted much attention for new generation opto-electronic applications due to their broad transparency from visible to infrared region, high solubility of rare-earth ions and good non-linear optical properties [1-11]. Recently, antimony oxide-based glasses have emerged as one major family of heavy metal

oxide glasses and appeared promising for potential applications in non-linear optical devices like ultra-fast optical switches and power limiters [2-5,12]. They also have potential for broad band optical amplifiers operating around 1.5 mm as antimony-silicate glass fibers and in the field of optical amplification in telecommunication C-band (1530 - 1560 nm) [1,13]. Antimonite glasses possess low phonon energy (605 $cm^{-1}$) and large optical non-linearity that is correlated to high refractive index, good mechanical properties and better chemical durability than that of fluoride or tellurite glasses [1-6,14,15].

The incorporation of $Sb_2O_3$ with conventional glass formers enhances vitrification behavior but also increases the phonon energy which leads to reduced infrared transmission. Numerous $Sb_2O_3$-based binary and multi-component glasses including conventional glass formers have been reported in the literature [1,16-21]. Therefore, recently alkali antimonite glasses free of conventional glass formers have been the subject of some studies in different systems such as; $Sb_2O_3$-$Na_2O$-ZnO, $Sb_2O_3$-$M_2O$-$MoO_3$ (where M = Li, K), $Sb_2O_3$-$Li_2O$-$GeO_2$, $Sb_2O_3$-$Na_2O$-$WO_3$-$Bi_2O_3$, $Sb_2O_3$-$M_2O$-PbO (where M = Li, Na or K), $Sb_2O_3$-$Na_2O$-$WO_3$ and $Sb_2O_3$-$Na_2O$-$Al_2O_3$ [1-5,14,15,22-25].

The aim of this work is to study new quaternary antimonite glasses in the $Sb_2O_3$-$Na_2O$-$WO_3$-PbO system. PbO and $WO_3$ have been introduced since they increase refractive index hence yield suitable glasses for non-linear applications.

In order to develop new glasses for opto-electronic applications, the knowledge of physical features of these glasses in combination with their thermal and structural properties seems to be a useful tool for understanding the glass structure. In this paper, to the best of our knowledge, we report for the first time on the glass formation behavior and thermal, physical and structural properties of glasses in the $Sb_2O_3$-$Na_2O$-$WO_3$-PbO glass system.

## 2. Experimental procedures

### 2.1. Glass synthesis

In order to prepare and characterize new antimony oxide-based multicomponent heavy metal oxide glasses, high purity chemicals of $Sb_2O_3$ (Acros, 99.99%), PbO (Aldrich, 99.9%), $WO_3$ (Aldrich, 99.995%) and $Na_2CO_3$ (Aldrich, 99.99%) were used as starting materials in the $Sb_2O_3$-$Na_2O$-$WO_3$-PbO quaternary glassy system. The synthesis was carried out through conventional melt-quenching method in open silica glass crucibles with 15 mm in diameter. After weighing and thoroughly mixing, batches of 5 g in weight were flame heated at a temperature close to 900 °C for 10 to 15 minutes in air. During the synthesis, the tube was shaken to homogenize the melt, while a release of $CO_2$ was observed due to the decomposition of sodium carbonate to sodium oxide. Vitreous samples were obtained by pouring the melt onto brass molds. The samples were annealed near the glass transition temperature for 6 hours in order to erase their thermal history. Finally, the samples were cut and polished. For different physical measurements, a set of samples were prepared according to the following composition rule: $x$$Sb_2O_3$-10$Na_2O$-$y$$WO_3$-$z$PbO, $z$ varying between 10 and 40 (mol %), the ratio of $x/y$=6 is maintained constant and $x+y+z$=90. Compositions of the prepared glass samples are given in Table 1 with their sample ID's.

To assess the residual silicon ($SiO_2$) arising from crucible contamination in the prepared glasses, semi quantitative analysis was performed using scanning electron microscopy / energy dispersive X-ray spectroscopy (SEM / EDS) techniques in JEOL Model JSM 6400 microscope linked with Oxford link ISIS energy dispersive X-ray spectrometer. The EDS measurements on glass samples were done at four different points for each glass composition.

The amorphous nature of the as-cast samples was checked by X-ray diffraction analysis (XRD) using Cu Kα radiation PANalytical/Philips X'pert MRD system, at 40KV and 40mA in the 2θ range from 10° to 90°.

2.2. Thermal investigations

Thermal properties of glasses was investigated by using differential scanning calorimetry analysis (DSC) in a Netzsch DSC 204 F1 (limit of detection: <0.1 μW, with an error estimate of ± 1 °C) using a constant sample weight of 25 ± 1 mg in aluminum pans, under flowing (25 ml/min) argon gas with a heating rate of 10 °C/min to determine the glass transition onset ($T_g$), first crystallization onset ($T_{c1}$) and first crystallization peak ($T_{p1}$) temperatures. The temperature difference between the glass transition onset ($T_g$) and the first exothermic peak onset ($T_{c1}$), $\Delta T = T_{c1} - T_g$, indicating the value of glass stability against crystallization was calculated.

The activation energy of the glass transition reaction, $E_g$, was determined by running non-isothermal DSC scans of the glasses at different heating rates, $\beta$, (10, 20, 30 and 40 °C/min). The activation energy values were calculated from the slopes of the linear fits to the experimental data from a plot of $\ln(T_g^2/\beta)$ versus $1/T_g$ by using the modified Kissinger equation [26]:

$$\ln\left(\frac{T_g^2}{\beta}\right) = \frac{E_g}{RT_g} + const \tag{1}$$

where $T_g$ is the glass transition onset temperature for a given heating rate $\beta$, $E_g$ is the glass transition activation energy and $R$ is the gas constant.

The fragility parameter, $m$, of the glasses was calculated (with an error estimate of ± 1) using the following expression [27,28]:

$$m = \left(\frac{E_g}{RT_g}\right) \tag{2}$$

where $m$ is the fragility parameter, $E_g$ is the activation energy for glass transition, $T_g$ is the glass transition onset temperature and $R$ is the gas constant.

2.3. Physical investigations

Physical properties of glasses were investigated by measuring the densities of glasses and calculating the molar volume, oxygen molar volume and oxygen packing density values.

Theoretical density values of glasses were determined by using the theoretical densities of the constituent oxides according to their appropriate concentrations. Densities, $\rho$, of the glasses were determined at room temperature by the Archimedes' method using ethanol as an immersion liquid and a digital balance of sensitivity $10^{-4}$ g. Density values obtained by three repeated measurements showed an error of ± 0.1 %. Density values of glasses, $\rho_{glass}$, were calculated using the following relation:

$$\rho_{glass} = \frac{W_{air}}{(W_{air} - W_{water})} \tag{3}$$

where $W_{air}$ and $W_{water}$ are the weight of the glass sample in air and in distilled water, respectively [29].

Molar volume of the glasses, $V_M$, was calculated as a function of the molar fraction of each component, using the relation:

$$V_M = \frac{M_{glass}}{\rho_{glass}} = \frac{\sum x_i M_i}{\rho_{glass}} \tag{4}$$

where $x_i$ is the molar fraction of each component $i$, $M_i$ is the molecular weight and $\rho$ density of the glass sample [29].

Oxygen molar volume of the glasses, $V_O$, was calculated using the following formula:

$$V_O = \left( \sum \frac{x_i M_i}{\rho} \right) \left( \frac{1}{\sum x_i n_i} \right) \tag{5}$$

where $x_i$ is the molar fraction of each component $i$, $M_i$ is the molecular weight and $\rho$ density of the glass sample and $n_i$ is the number of oxygen atoms in each constituent oxide [29,30].

Oxygen packing density of the glasses, OPD, was calculated using the density and composition values by applying the following formula:

$$OPD = 1000C(\rho / M) \quad (6)$$

where $C$ is the number of oxygen atoms per each composition, $\rho$ is the density and $M$ is the molecular weight of the glass sample [29,30].

The refractive index of glasses was measured using a Metricon M2010 at four different wavelengths (632.8, 825, 1060.7 and 1551 nm) with an accuracy of ± $1.10^{-4}$.

The transmittance spectra of glasses were measured onto polished samples by a Perkin Elmer Lambda 1050 UV-Vis-NIR spectrophotometer operating between 400 and 800 nm, with 2 nm resolution. The wavelength, $\lambda_g$, corresponding to the optical band gap, $E_g$, is given when the absorption of the glass reaches 10 $cm^{-1}$ [5]. The absorption coefficient is calculated according to the following equation:

$$\alpha = \frac{1}{x} ln\left(\frac{T_{max}}{T}\right) \quad (7)$$

where T and $T_{max}$ are the transmittance and maximum transmittance, respectively and $x$ is the sample thickness. Then, $E_g$ values (in eV) were calculated using the following equation:

$$E_g = \frac{hc}{\lambda_g} \quad (8)$$

where $h$ represents the Planck constant and $c$ is the speed of light.

2.3. Structural investigations

Quantitative analysis of thermal and physical properties of these glasses with structural parameters like average cross-link density, number of bonds per unit volume and Poisson's ratio were also studied.

Average cross-link density, $\overline{n_c}$, of the glasses was calculated using the subsequent relation:

$$\overline{n_c} = \frac{\sum_i x_i (n_c)_i (N_c)_i}{\sum_i x_i (N_c)_i} \quad (9)$$

where $x_i$ is the molar fraction of each component, $n_c$ is the cross-link per cation and $N_c$ is the number of cations per glass formula unit [29,31].

Number of bonds per unit volume of the glasses, $n_b$, was calculated by applying the following formula:

$$n_b = \frac{N_A}{V_M}\sum_i (n_f x)_i \tag{10}$$

where $N_A$ is the Avogadro's number, $V_M$ molar volume of the glass sample, $n_f$ coordination number of the cations, $x$ molar fraction of each component oxide and $i$ represents the component oxide [29,31].

For Eq. 9 and 10, the cross-link per cation ($n_c$) is calculated as follows, $n_c = n_f - 2$, where $n_f$ is the coordination number of the cations, which equals 6 for $WO_3$, 4 for $Na_2O$ and PbO and 3 for $Sb_2O_3$, respectively [31,32].

Poisson's ratio of the glasses, $\mu_{cal}$, was calculated theoretically according to the following expressions:

$$\mu_{cal} = 0.5 - \frac{1}{7.2V_t} \tag{11}$$

$$V_t = \frac{\rho}{M}\sum_i x_i V_i \tag{12}$$

$$V_i = \frac{4\pi N_A}{3}(nr_A^3 + mr_O^3) \tag{13}$$

where $V_t$ is the packing density, $\rho$ density and $M$ molecular weight of the glass sample, $V_i$ packing factor of the oxide $A_nO_m$, $N_A$ Avogadro's number, $r_A$ and $r_O$ are the ionic radius of cation $A$ and anion $O$, respectively [29,31].

FTIR spectra of the glasses were collected at room temperature using CsI pellet technique in the range 1200 - 250cm$^{-1}$ with a resolution of 1 cm$^{-1}$ using a Perkin Elmer Frontier

FTIR spectrometer. For the FTIR experiments 0.005 g of glasses were weighed, mixed and ground with 0.5 g CsI, then the mixture was pressed at 15 tons for 1 minute to yield transparent disks suitable for mounting in the spectrometer.

**3. Results and discussion**

The samples prepared in the $Sb_2O_3$-$Na_2O$-$WO_3$-PbO system are amorphous as it was proven by XRD analysis.

The EDS analysis realized to check the elemental analysis of glasses and to assess the residual silicon arising from crucible contamination. Concentrations of all different elements in glasses are expressed in cation % and are listed in Table 2. The Si introduction in glasses is less than 3.22 cation % and increased in the range 0.09, 1.37, 2.51 and 3.22 cation % with increasing PbO concentration from *x*=10, 20, 30 to 40 mol % respectively. The increase in the Si ratio can be related firstly to the increase in melting time needed to homogenize the melt when the PbO concentration increases in the glass and secondly to the increase in the melting temperature of the melt when the PbO ratio increases. Considering that the melting temperature of individual antimony, tungsten, lead and sodium oxides are 656, 1473, 888 and 851°C respectively and the mean melting temperature of the glass batch varies between 850 and 880 °C, the used melting temperature of 900°C is sufficient to achieve the melting procedure. Chemical analysis of glass samples is in good agreement with the compositions determined from weighed starting batch materials. Volatilization during melting is limited and the deviation from the nominal composition is less than 1.5%.

It should be noted that the concentration of $Na_2O$ in $Sb_2O_3$-$Na_2O$-$WO_3$-PbO glasses is maintained constant and equals to 10 mol %. However, in fact the ratio of $Na_2O$ in the glasses doesn't necessarily remain constant when the concentration of PbO increases from 10 to 40 mol %. A fourfold increase in the concentration of PbO at the same time leads to almost a twofold increase in the concentration of $Na_2O$. It is determined that $Na^+$ concentration changes from

11.2 to 13.08 cation % in the nominal composition and from 8.63 to 11.93 cation % in the real composition of the prepared glasses. This small change in the concentration of sodium is expected to have a small influence on different physical properties of these glasses and therefore the main influence can be related to the change in PbO concentration.

DSC analysis was performed to investigate the thermal properties of $Sb_2O_3$-$Na_2O$-$WO_3$-PbO glasses. Thermal analysis details of quaternary glasses are given in Table 1. The DSC curves of SNWP10, SNWP20, SNWP30 and SNWP40 glasses scanned at a heating rate of 10 °C/min are shown in Fig. 1. Each DSC scan exhibited a shallow endothermic change between 287 and 289 °C corresponding to the glass transition temperature ($T_g$) and large peaks between 375 and 500°C corresponding to the crystallization process. As can be seen from Table 1, $T_g$ values remain practically invariant with changing composition. However, first crystallization onset temperatures initially showed an increase by increasing PbO concentration to 20 mol% and then decreased with further increase of lead oxide concentration. The temperature difference between $T_g$ and the first exothermic peak onset $T_{c1}$, $\Delta T$, indicating the glass stability against crystallization was found to vary between 73 and 115 °C and the most stable glass composition with a maximum $\Delta T$ value was found as SNWP20 glass sample. It was observed that the change in $\Delta T$ with increasing PbO concentration showed a similar behavior to the change observed in first crystallization onset temperatures (see Fig. 1).

The heating/cooling rate dependence of the glass transition temperature is used to determine the activation energy of the transition from glassy to liquid state.

As can be seen from Fig. 2, using the modified Kissinger equation (Eq. (1)), activation energy of the glass transition, $E_g$, for $Sb_2O_3$-$Na_2O$-$WO_3$-PbO glasses were determined from the linear fits of $\ln(T_g^2/\beta)$ versus $1000/T_g$ plots. As shown in Fig. 2, activation energy of the glass transition increased with increasing PbO concentration from 330 kJ/mol to 412 kJ/mol (see also Table 1). A rough estimate of deviation of activation energies were calculated applying R×

$SE_{slope}$; R being the ideal gas constant and $SE_{slope}$ being the standard deviation of the slope obtained from linear regression and it was found that activation energies of $Sb_2O_3$-$Na_2O$-$WO_3$-PbO glasses showed an error of 16.7, 32,6, 35.9 and 39.5 kj/mol with increasing PbO concentration, respectively. As it was reported in the literature, the bond energies of Sb–O, W–O and Pb–O are 372 kJ/mol, 378 kJ/mol and 653 kJ/mol respectively and the increase in $E_g$ values in $Sb_2O_3$-$Na_2O$-$WO_3$-PbO glasses with increasing PbO concentration is attributed to the increase in coordination number [33-37].

The values of fragility parameter, *m*, which is often used to determine the strong-fragile characters of glass forming liquids, are listed in Table 1. Fragility parameters, *m*, of $Sb_2O_3$-$Na_2O$-$WO_3$-PbO glasses were found to vary between 70 and 87 and showed an increase with increasing PbO concentration. It is known from the literature that there is no sharp limit to characterize strong-fragile characters of liquids on the basis of their fragility parameters. However, it is mentioned that a fragility value less than 90 can be attributed for strong liquids, whereas a value greater than 135 is typical for fragile liquids [27]. By taking this into account, it can be concluded that $Sb_2O_3$-$Na_2O$-$WO_3$-PbO glasses have a strong character and increasing the PbO concentration leads a less strong character. Therefore, it can be stated that the viscosity and heat capacity values of these glasses show a small change in the glass transition region [27,28,33].

Physical properties of the glasses were investigated by measuring the density, $\rho$, molar volume $V_M$, oxygen molar volume, $V_O$ and oxygen packing density, OPD values to throw light on the structural behavior of $Sb_2O_3$-$Na_2O$-$WO_3$-PbO glasses and the obtained values are given in Table 1.

Densities of $Sb_2O_3$-$Na_2O$-$WO_3$-PbO glasses varied between 5.31 and 5.68 g/cm$^3$ and showed an increase with increasing PbO concentration. Densities of glasses determined at room temperature were found to be consistent with their theoretical values. The increase in density

with increasing PbO concentration is due to the higher density of PbO among other constituent oxides. Molar volume values were calculated by taking into account the measured densities and they were found to vary between 48.01 and 41.72 $cm^3$/mol. Molar volume values exhibited a decrease with increasing PbO concentration. The decrease in molar volume values with increasing PbO concentration is due to the decrease in the percentage of oxygen atoms which have the highest ionic radius in the glass structure ($O^{2-}$: 0.14nm, $Sb^{3+}$: 0.076nm, $W^{6+}$: 0.065nm, $Pb^{2+}$: 0.119nm) [29,38]. Therefore, it can be stated that decreasing oxygen content in glass composition decreases the excess free volume by decreasing the molar volume. Fig. 3 demonstrates the variation of density and molar volume values with changing PbO molar concentration.

Oxygen molar volume values of $Sb_2O_3$-$Na_2O$-$WO_3$-PbO glasses showed a change between 31.55 and 31.92 $cm^3$/mol and increased slightly with increasing PbO concentration. On the other hand, oxygen packing density values varied between 54.16 and 47.94 mol/l and showed a decrease with increasing PbO concentration. Variation of oxygen molar volume and oxygen packing density values of $Sb_2O_3$-$Na_2O$-$WO_3$-PbO glasses is illustrated in Fig. 4. As it can be seen from Fig. 4, oxygen molar volume and oxygen packing density values show opposite behavior to each other. Therefore, it can be concluded that due to the substitution of higher field intensity constituent ions ($Sb^{3+}$: 0.73, $W^{6+}$: 1.47) with lower field intensity $Pb^{2+}$ ions (0.27) [29,39,40] a slight increase in oxygen molar volume and a decrease in oxygen packing density values were observed in $Sb_2O_3$-$Na_2O$-$WO_3$-PbO glasses which results less tightly packing of the glass network.

The measured refractive indices in the $Sb_2O_3$-$Na_2O$-$WO_3$-PbO system were found to vary between 2.0 and 2.1 depending on wavelength and composition (Table 3). For each glass sample the increase of the density implies the increase of the refractive index. Therefore, it was

observed that the density, and together with it the refractive index, both show an increase with increasing concentration of lead oxide (Fig. 5).

The transmittance spectra of $Sb_2O_3$-$Na_2O$-$WO_3$-PbO glasses are illustrated in Fig. 6. The short wavelength absorption edge is located at around 450 nm, hence the glasses have a light yellow color. The positions of the short wavelength absorption edge depend slightly on the glass composition with increasing PbO concentration and practically remained invariant. As it can be seen from Table 1, $E_g$ values initially showed a decrease from 2.979 to 2.972 eV by increasing the PbO concentration to 20 mol % and then linearly increased with further increase of PbO concentration.

In glasses, generally the addition of alkali oxides, alkaline earth oxides and many other divalent metal oxides like PbO causes depolymerization in the glass network by breaking chains to create non-bridging oxygens (NBOs). Consequently, any changes in the oxygen bonding in a glass network, such as the formation of NBOs will also result in changes in the absorption characteristics. The NBOs, which bound an excited electron less tightly than the bonded oxygens (BOs), are more polarizable than the BOs. Thus, creation of NBOs seems to be the reason for the decrease in $E_g$ values when PbO content increased from 10 to 20 mol %. In this case PbO plays the role of glass modifier by forming [$PbO_6$] units to repair the balance charge of two NBOs induced by two alkali ions like $Na^+$. The increase in $E_g$ for PbO concentrations more than 20 mol% may indicate the decrease in the NBOs. In this case PbO is supposed to play a former role by forming [$PbO_3$] or [$PbO_4$] units.

In order to interpret thermal and physical properties of $Sb_2O_3$-$Na_2O$-$WO_3$-PbO glasses thoroughly, structural properties were investigated by calculating average cross-link density, $\overline{n_c}$, number of bonds per unit volume, $n_b$, and Poisson's ratio, $\mu_{cal}$, and the obtained results are given in Table 1.

Average cross-link density values decreased from 2.21 to 2.13 with increasing PbO concentration. The decrease in average cross-link density with increasing PbO concentration implies that the addition of PbO to antimonite glasses decrease the network connectivity by creating non-bridging oxygen sites.

Number of bonds per unit volume varied between 75.24 and 77.92 x $10^{21}$ $cm^{-3}$ and showed an increase with the increase in PbO concentration. The theoretically calculated Poisson's ratio values varied between 0.174 and 0.158 and decreased with increasing PbO concentration. The increase in number of bonds per unit volume and decrease in calculated Poisson's ratio with the increase in PbO concentration yields a rigid and more linked glass network.

FTIR spectra in the spectral range [1200-250$cm^{-1}$] of $Sb_2O_3$-$Na_2O$-$WO_3$-PbO glasses for increasing PbO concentration are shown in Fig. 7. In general, FTIR spectra of glasses showed broad peaks and shoulders due to the disorder of the glass structure.

$Sb_2O_3$ exists in two crystalline forms: cubic senarmontite and orthorhombic valentinite. Antimony oxide is a weak glass network former and does not form glass without the presence of modifiers with $SbO_3$ triangular pyramids. Sb participates in the glass network with the oxygen at three corners and the lone pair of electrons of antimony at the fourth corner. Crystalline $Sb_2O_3$ exhibits four fundamental absorption bands: symmetric stretching vibrations ν1 (925 $cm^{-1}$), symmetric bending vibrations ν2 (600 $cm^{-1}$), doubly degenerate stretching vibrations ν3 (710 $cm^{-1}$) and doubly degenerate bending vibrations ν4 (485 $cm^{-1}$). The network structure of the glass is found to be double chains consisting of four membered rings of $SbO_3$ pyramids similar to the valentinite form [21,41-43]. As reported in the literature, during synthesis of glasses at high temperatures, small part of $Sb^{3+}$ (in $Sb_2O_3$ used as the raw material) is expected to convert to $Sb^{5+}$ by accepting oxygen from air due to its multivalent

characteristics. These $Sb^{5+}$ ions enter to the glass structure as singly positive $[SbO_4]^{4-}$ coordinated units [43].

The spectra for $Sb_2O_3$-$Na_2O$-$WO_3$-PbO glasses are dominated by four main bands centered at around 470, 594, 700 and 937 $cm^{-1}$ in the fingerprint range of 400-1200 $cm^{-1}$. The IR bands at 470 and 594$cm^{-1}$ correspond to the ν4 and ν3 vibration modes of $SbO_3$ of the valentinite form of $Sb_2O_3$ as reported by Terashima et al. [42]. The band located at 700$cm^{-1}$ can be assigned to the ν1 vibration mode and the band at 937$cm^{-1}$ is due to the Si–O stretching vibration of $SiO_4$ tetrahedra. These bands were due to the contamination from the silica crucible used for melting the glasses as confirmed by EDS analysis. The presence of bands related to $Sb^{5+}$ is not confirmed in these glasses.

According to the literature, PbO has the ability to form stable glasses due to its dual role in glass structure. When PbO introduced to the glass structure as a modifier, Pb–O binding has an ionic character and observed in the range 400-200 $cm^{-1}$, whereas as a glass former Pb–O binding is covalent and observed in the range 600-400 $cm^{-1}$. In the latter case, Pb ions create three-dimensional spatial network with $[PbO_4]$ or $[PbO_3]$ units. This fact is possible for glasses having high amounts of PbO (more than 50 mol %) [32]. Accordingly, as can be seen from Fig. 7, the band located in the far infrared spectra at 290 $cm^{-1}$ can be assigned to the ionic bands of Pb–O. The intensity of this band decrease with increasing PbO concentration and for SNWP30 and SNWP40 glasses two new bands appear at 350 $cm^{-1}$ and 450 $cm^{-1}$ which can be assigned to the vibrational mode of covalent bonds in $[PbO_4]$ or $[PbO_3]$ units.

In our previous study [44], it was observed that the equimolar substitution of $Sb_2O_3$ with PbO reduces the elastic properties in ternary glasses (90-*x*)$Sb_2O_3$-10$Na_2O$–*x*PbO (for *x*=10-40) by creating weak Sb–O–Pb bonds. These weak bonds can be the consequence of the presence of the band situated at 812 $cm^{-1}$ (see Fig. 7). Its intensity increases with increasing PbO concentration which excludes the possibility of assigning this band to W–O vibrations. In the

same order, the remarkable shift of the asymmetric stretching vibration of [$SbO_3$] units from 594 to 580 $cm^{-1}$ can be caused by the presence of weak bonds corresponding to Sb–O–Pb linkages. The incorporation of $WO_3$ in glasses generally induces the appearing of two shoulders at around 700-800 and 800-860 $cm^{-1}$ which are attributed to W–O–W vibration modes and a well-defined band in the 905-930 $cm^{-1}$ range corresponding to the vibration mode of W–O in the tetrahedral [$WO_4$] or octahedral [$WO_6$] units [39]. In the FTIR spectra given in Fig. 7, a weak shoulder at 913 $cm^{-1}$ confirmed the presence of tungstate units in $Sb_2O_3$-$Na_2O$-$WO_3$-PbO glasses. The decrease of $WO_3$ concentration in the glass structure induces a shift of this band from 913 to 893 $cm^{-1}$. This shift was attributed to the change of tungsten coordination from [$WO_6$] to [$WO_4$] units which is in good agreement with the diminution of oxygen packing density of the glasses with increasing PbO concentration [45].

In summary, PbO enters the glass structure as a glass modifier and increasing the PbO concentration by keeping the $Sb_2O_3/WO_3$ ratio constant leads to the formation of lead structural units and favors the former role at the expense of modifying role.

**4. Conclusions**

In this experimental work, thermal, physical and structural properties of new heavy metal oxide glasses in the $Sb_2O_3$-$Na_2O$-$WO_3$-PbO system were investigated. Thermal investigations reveal that the glass transition values remained practically invariant with changing composition, while the first crystallization onset temperatures initially showed an increase with increasing PbO concentration and then decreased. Kinetic investigations of glass transition region showed that activation energy of glass transition values increased with increasing PbO concentration due to the increase in coordination number. Kinetically estimated fragility values show that $Sb_2O_3$-$Na_2O$-$WO_3$-PbO glasses have a strong character. Physical and structural investigations revealed that increasing PbO concentration in glass structure results a decrease in molar volume, oxygen packing density, average cross-link density and calculated

Poisson's ratio values and on the contrary results an increase in the density, refractive index, oxygen molar volume and number of bonds per unit volume. Taking these into account, it can be concluded that increasing PbO concentration decreases the network connectivity of quaternary antimonite glasses by creating non-bridging oxygen sites which also results less tightly packing of the glass network. However, the FTIR results suggest the presence of both modifier and former role of PbO in these glasses.

**References**


[1] K. Ouannes, M.T. Soltani, M. Poulain, G. Boulon, G. Alombert-Goget, Y. Guyot, A. Pillonnet, K. Lebbou, J. Alloys Compd. 603 (2014) 132-135.

[2] J. Zavadil, Z.G. Ivanova, P. Kostka, M.Hamzaoui, M.T. Soltani, J. Alloys Compd. 611 (2014) 111-116.

[3] M.T. Soltani, M. Hamzaoui, S. Houhou, H. Touiri, L. Bediar, A.M. Ghemri, P. Petkova, Acta Phys. Pol. A 123 (2013) 227-229.

[4] M. Hamzaoui, S. Azri, M.T.Soltani, R.Lebullenger, M. Poulain, Phys. Scr. T157 (2013) 014029.

[5] M. Baazouzi, M.T. Soltani, M. Hamzaoui, M. Poulain, J. Troles, Opt. Mater. 36 (2013) 500-504.

[6] M.T. Soltani, A. Boutarfaia, R. Makhloufi, M. Poulain, J. Phys. Chem. Solids 64 (2003) 2307-2312.

[7] D. Lezal, J. Pedlikova, P. Kostka, J. Bludska, M. Poulain, J. Zavadil, J. Non-Cryst. Solids 284 (2001) 288-295.

[8] P. Kostka, J. Zavadil, J. Pedlikova, M. Poulain, Phys. Status Solidi A 208 (2011) 1821-1826.

[9] M. Nouadji, Z.G. Ivanova, M. Poulain, J. Zavadil, A. Attaf, J. Alloys Compd. 549 (2013) 158-162.

[10] L. Żur, M. Sołtys, J. Pisarska, W.A. Pisarski, J. Alloys Compd. 578 (2013) 512-516.

[11] M. Çelikbilek, A.E. Ersundu, S. Aydin, J. Am. Ceram. Soc. 96 (2013) 1470-1476.

[12] R.E. de Araujo, C.B. de Araujo, G. Poirier, M. Poulain, Y. Messaddeq, Appl. Phys. Lett. 81 (2002) 4694-4696.

[13] J. Minelly, A. Ellison, Opt. Fiber Tech. 8 (2002) 123-138.

[14] M. Hamzaoui, M.T. Soltani, M. Baazouzi, B. Tioua, Z.G. Ivanova, R. Lebullenger, M. Poulain, J. Zavadil, Phys. Status Solidi B 249 (2012) 2213-2221.

[15] P. Petkova, H. Touiri, M.T. Soltani, Acta Phys. Pol. A 123 (2013) 205-206.

[16] K. Biswas, B. Sathravada, G. Debarat, A.D. Sontakke, K. Annapurna, J. Alloys Compd. 608 (2014) 266-271.

[17] H. Nasu, S. Ninagawa, K. Inoue, T. Hashimoto, A. Ishihara, J. Ceram. Soc. Jpn. 120 (2012) 436-437.

[18] M. Nouadji, A. Attaf, R. El Abdi, M. Poulain, J. Alloys Compd. 511 (2012) 209-214.

[19] Q. Qian, Y. Wang, Q.Y. Zhang, G.F. Yang, Z.M. Yang, Z.H. Jiang, J. Non-Cryst. Solids 354 (2008) 1981-1985.

[20] B. Zhang, Q. Chen, L. Song, H. Li, F. Hou, J. Zhang, J. Non-Cryst. Solids 354 (2008) 1948-1954.

[21] S.Y. Marzouk, F.H. Elbatal, J Mol. Struct. 1063 (2014) 328-335.

[22] R. Vijay, P. Ramesh Babu, B.V. Raghavaiah, P.M. Vinaya Teja, M. Piasecki, N. Veeraiah, D. Krishna Rao, J. Non-Cryst. Solids 386 (2014) 67-75.

[23] P. Petkova, M.T. Soltani, S. Petkov, J. Tacheva, V. Nedkov, Phys. Scripta T149 (2012) 014057.

[24] P. Petkova, S. Houhou, M.T. Soltani, Phys. Scripta T157 (2013) 014042.

[25] P. Petkova, H. Touiri, M.T. Soltani, Phys. Scripta T157 (2013) 014041.

[26] H.E. Kissinger, J. Res. Nat. Bur. Stand. 57 (1956) 217-221.

[27] D. Zhu, C.S. Ray, W. Zhou, D.E. Day, J. Non-Cryst. Solids, 319 (2003) 247-256.

[28] R. Brüning, M. Sutton, J. Non-Cryst. Solids 205-207 (1996) 480-484.

[29] M. Çelikbilek, A.E. Ersundu, S. Aydin, J. Non-Cryst. Solids 378 (2013) 247-253.

[30] A.E. Ersundu, M. Çelikbilek, N. Solak, S. Aydin, J. Eur. Ceram. Soc. 31 (2011) 2775-2781.

[31] I.Z. Hager, R.A.H. El-Mallawany, J. Mater. Sci. 45 (2010) 897-905.

[32] B.V. Raghavaiah, C. Laxmikanth, N. Veeraiah, Opt .Commun. 235 (2004) 341-349.

[33] A.E. Ersundu, M. Çelikbilek, S. Aydin, J. Non-Cryst. Solids 358 (2012) 641-647.

[34] T. L. Cottrell, The Strengths of Chemical Bonds, second ed., Butterworth, London, 1958.

[35] S. W. Benson, J. Chem. Educ. 42 (1965) 502-518.

[36] J. A. Kerr, Chem. Rev. 66 (1966) 465-500.

[37] B. deB. Darwent, Bond Dissociation Energies in Simple Molecules, National Standard Reference Data Series, Washington, 1970.

[38] R.D. Shannon, Acta Crystall. A-Crys.32, (1976) 751-767.

[39] D. Munoz-Martín, M.A. Villegas, J. Gonzalo, J.M. Fernández-Navarro, J. Eur. Ceram. Soc. 29 (2009) 2903-2913.

[40] T. Som, B. Karmakar, J. Mod. Optic 58 (2011) 1012-1023.

[41] G.L. Flower, G.S. Baskaran, N.K. Mohan, N. Veeraiah, Mater. Chem. Phys. 100 (2006) 211-216.

[42] K. Terashima, T. Hashimoto, T. Uchnio, S. Kim, T. Yoko, J. Ceram. Soc. Jpn. 104 (1996)1008-1014.

[43] T. Som, B. Karmakar, Antimony oxide glasses and their nanocomposites for optical, photonic and nanophotonic applications, in: Razeghi M. (Ed.), Antimony: Characteristics, Compounds and Applications, Nova Publishers, ebook, 2012, pp. 5-7.

[44] M.T. Soltani, T. Djouama, A. Boutarfaia, M. Poulain, J. Optoelectron. Adv. M. 1 (2009) 339-342.

[45] S. Al-Ani, C.A. Hogarth, R.A.H. El-Mallawany, J. Mater. Sci. 20 (1985) 661-667.

# FIGURE CAPTIONS

**Fig. 1.** DSC curves of $Sb_2O_3$-$Na_2O$-$WO_3$-PbO glasses, scanned at a heating rate of 10 °C/min.

**Fig. 2.** The Kissinger plots for determining glass transition, $E_g$ values of $Sb_2O_3$-$Na_2O$-$WO_3$-PbO glasses.

**Fig. 3.** Variation of density, ρ and molar volume, $V_M$ values of $Sb_2O_3$-$Na_2O$-$WO_3$-PbO glasses with PbO molar concentration.

**Fig. 4.** Variation of oxygen molar volume, $V_O$ and oxygen packing density, OPD values of $Sb_2O_3$-$Na_2O$-$WO_3$-PbO glasses with PbO molar concentration.

**Fig. 5.** Variation of refractive index of $Sb_2O_3$-$Na_2O$-$WO_3$-PbO glasses with PbO molar concentration at different wavelengths.

**Fig. 6.** Tranmittance spectra of $Sb_2O_3$-$Na_2O$-$WO_3$-PbO glasses.

**Fig. 7.** FTIR spectra of $Sb_2O_3$-$Na_2O$-$WO_3$-PbO glasses.

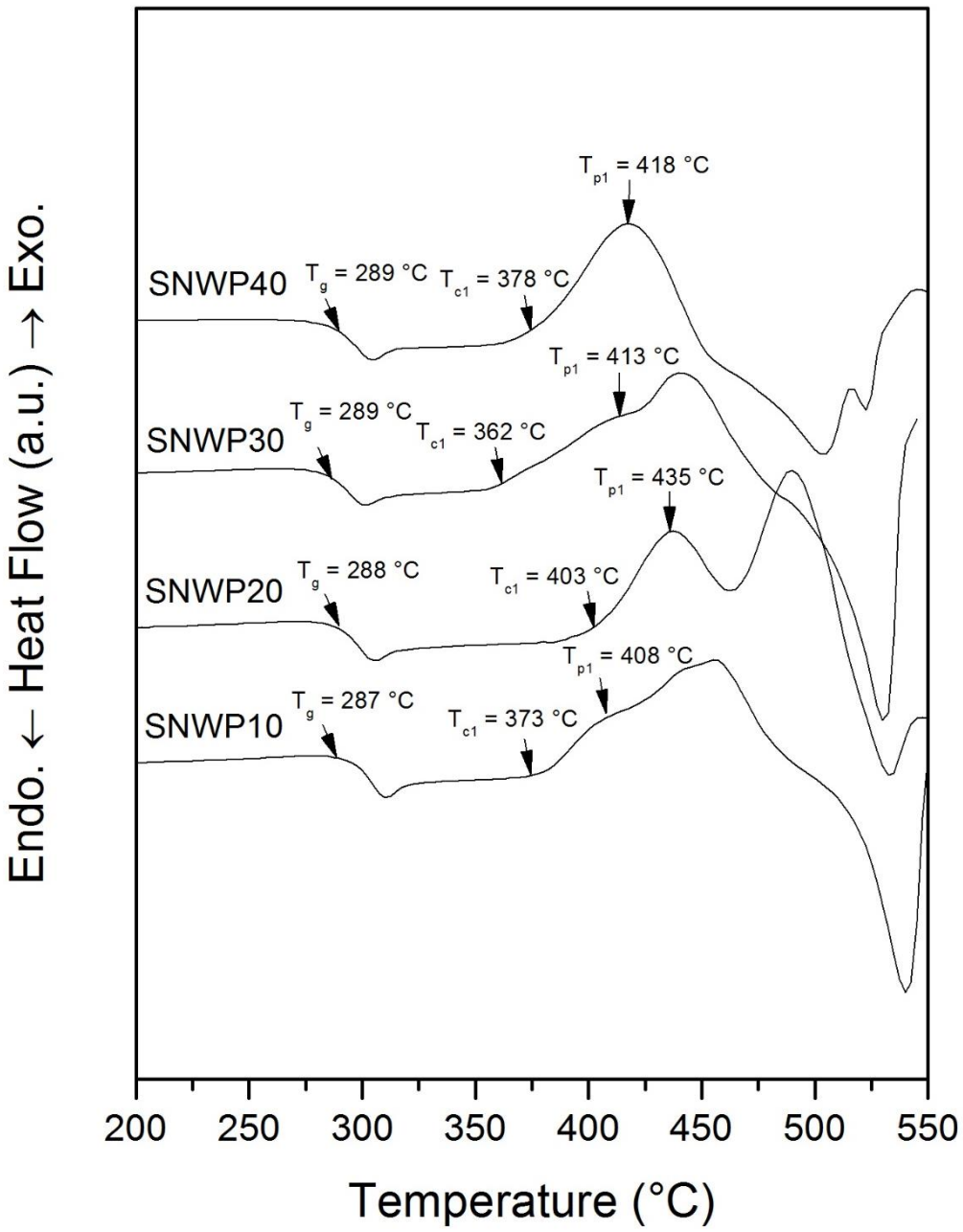
Endo. ← Heat Flow (a.u.) → Exo.
SNWP40
$T_g$ = 289 °C
$T_{c1}$ = 378 °C
$T_{p1}$ = 418 °C
SNWP30
$T_g$ = 289 °C
$T_{c1}$ = 362 °C
$T_{p1}$ = 413 °C
SNWP20
$T_g$ = 288 °C
$T_{c1}$ = 403 °C
$T_{p1}$ = 435 °C
SNWP10
$T_g$ = 287 °C
$T_{c1}$ = 373 °C
$T_{p1}$ = 408 °C
200
250
300
350
400
450
500
550
Temperature (°C)

**Fig. 1.**

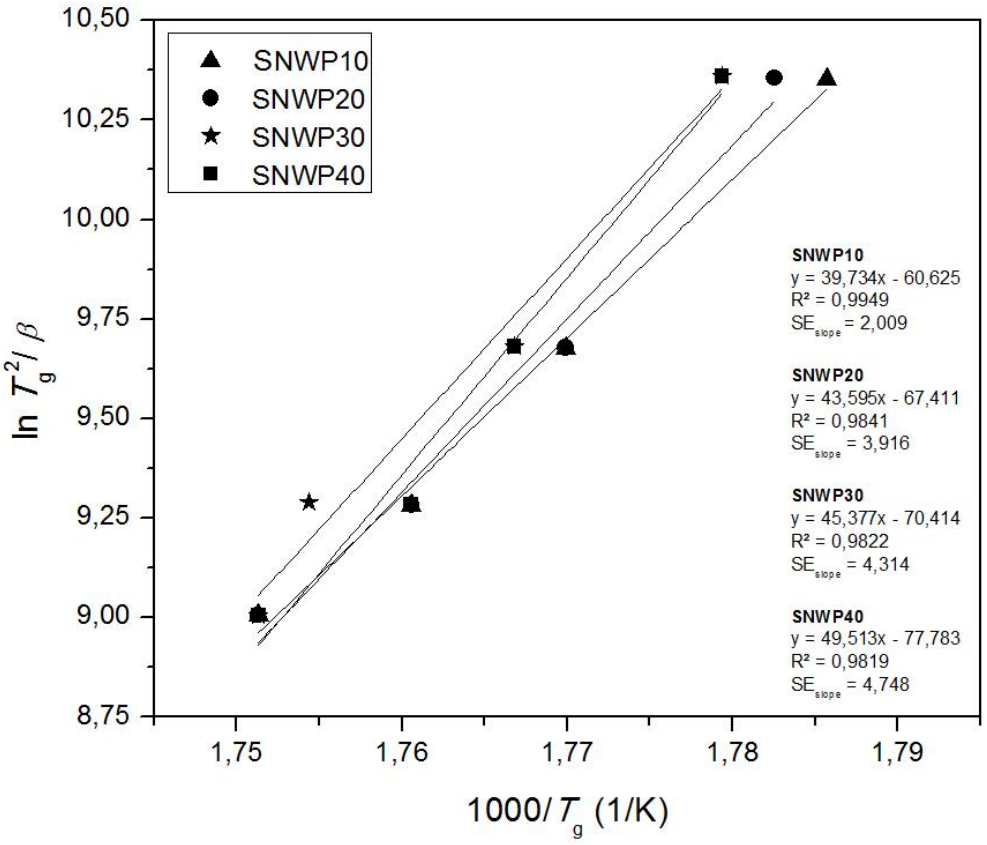
SNWP10
SNWP20
SNWP30
SNWP40
SNWP10
y = 39,734x - 60,625
R² = 0,9949
SE slope = 2,009
SNWP20
y = 43,595x - 67,411
R² = 0,9841
SE slope = 3,916
SNWP30
y = 45,377x - 70,414
R² = 0,9822
SE slope = 4,314
SNWP40
y = 49,513x - 77,783
R² = 0,9819
SE slope = 4,748
10,50
10,25
10,00
9,75
9,50
9,25
9,00
8,75
1,75
1,76
1,77
1,78
1,79
ln Tg2/ β
1000/ Tg (1/K)

**Fig. 2.**

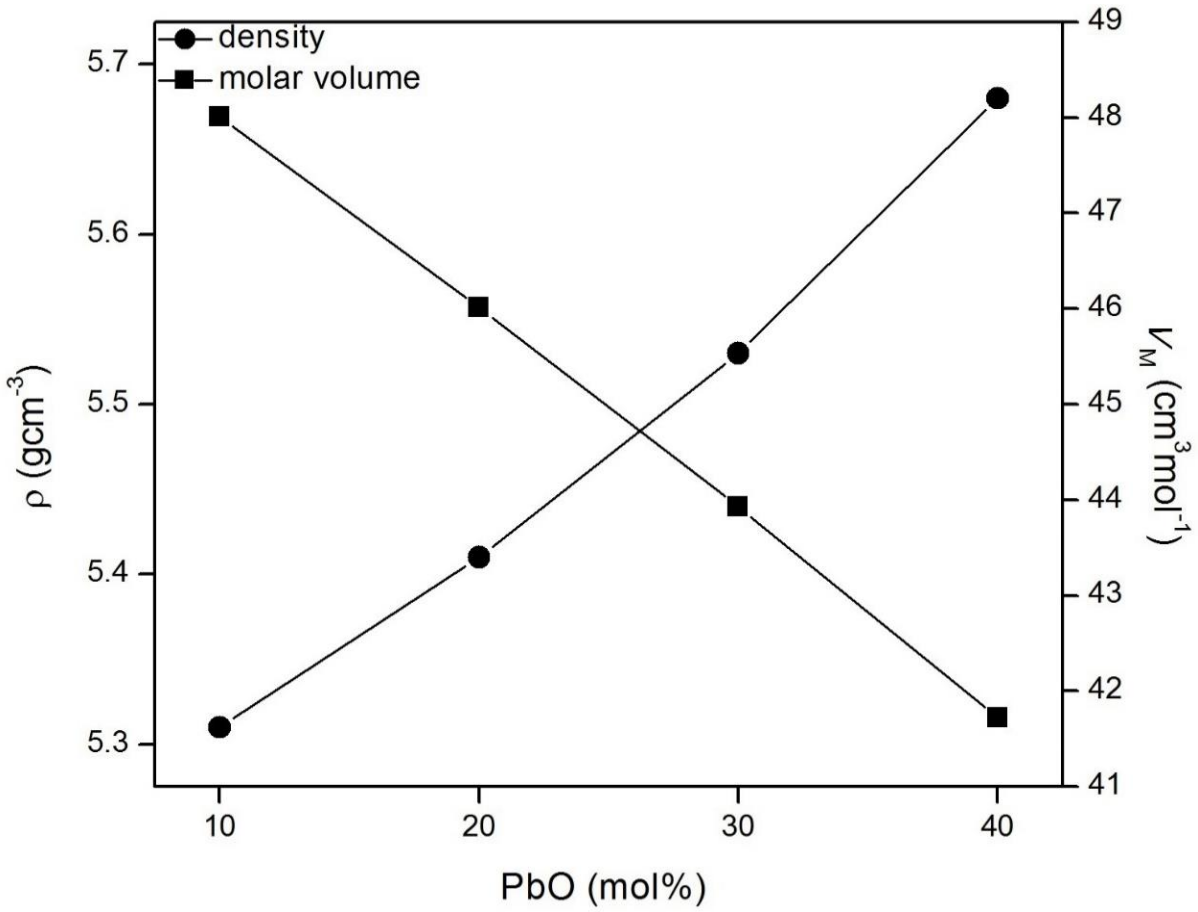
density
molar volume
5.7
5.6
5.5
5.4
5.3
ρ (gcm-3)
49
48
47
46
45
44
43
42
41
VM (cm3mol-1)
10
20
30
40
PbO (mol%)

**Fig. 3.**

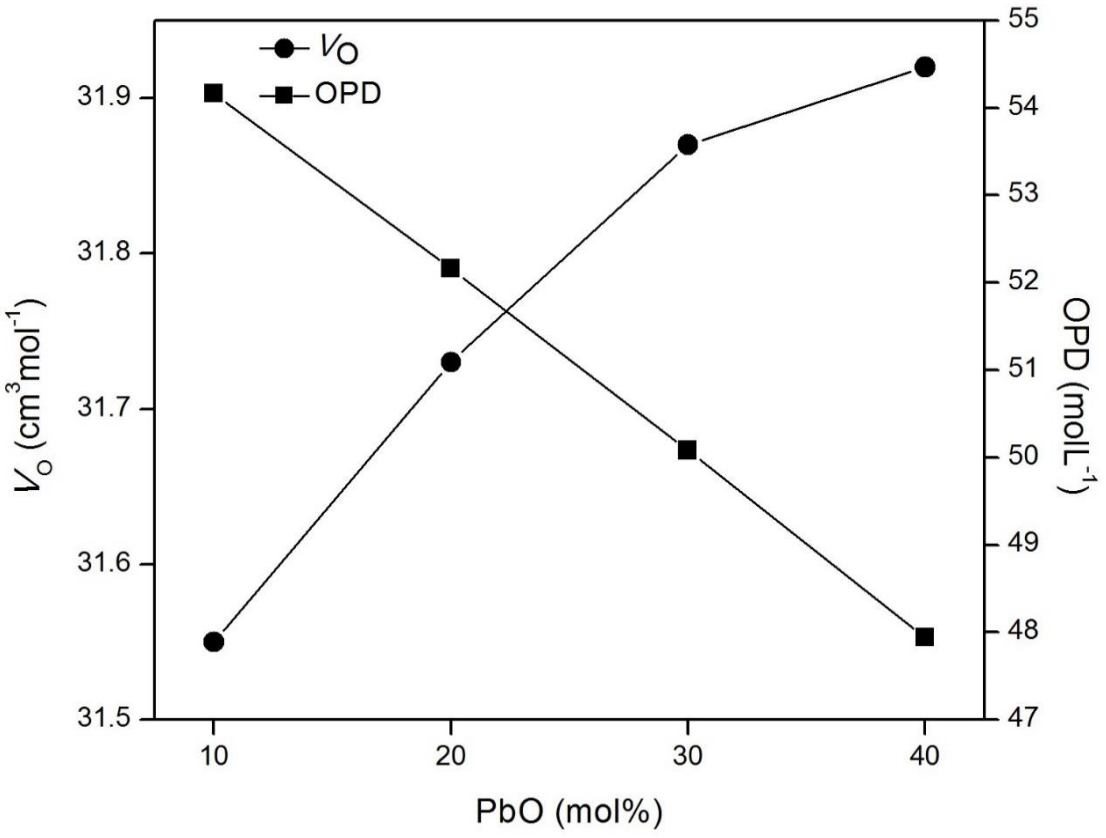
$V_O$
OPD
31.9
31.8
31.7
31.6
31.5
$V_O$ ($cm^3mol^{-1}$)
55
54
53
52
51
50
49
48
47
OPD ($molL^{-1}$)
10
20
30
40
PbO (mol%)

**Fig. 4.**

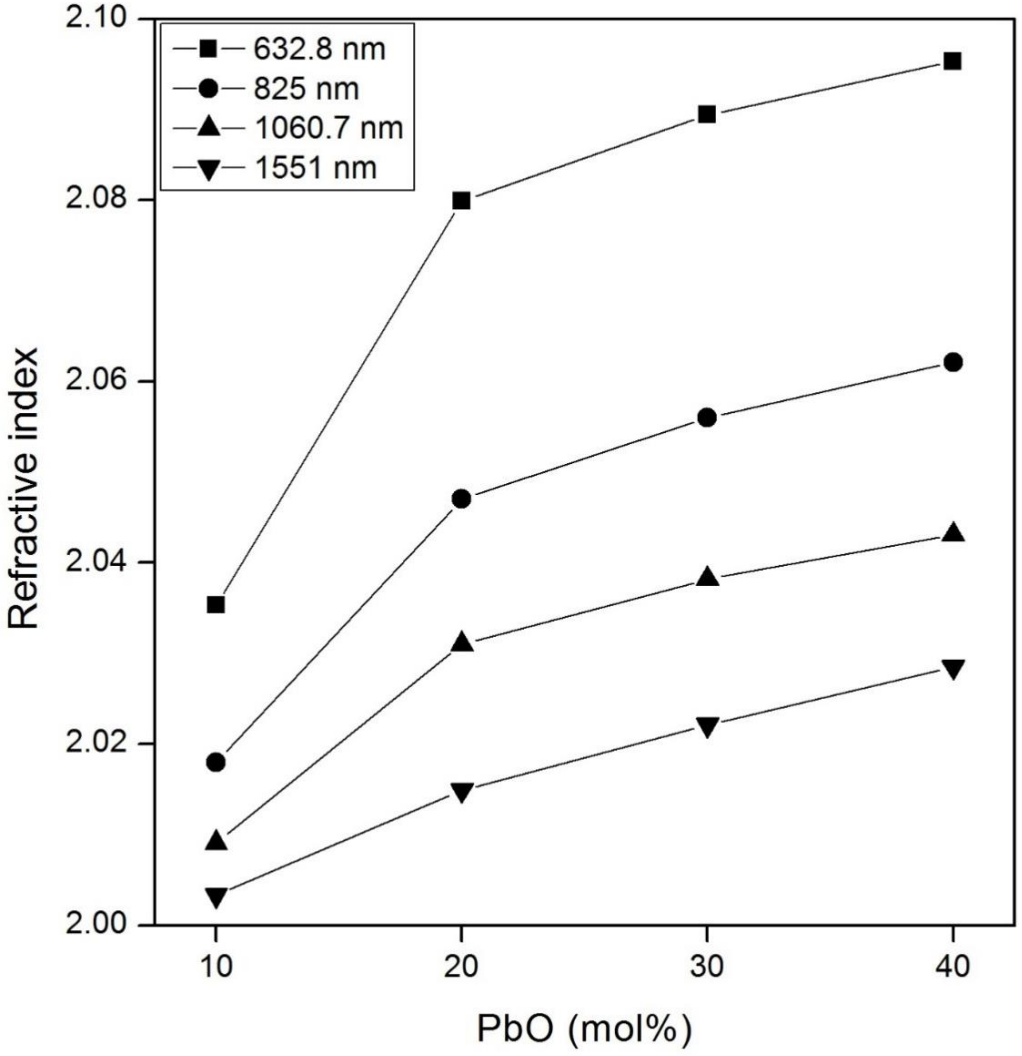
632.8 nm
825 nm
1060.7 nm
1551 nm
Refractive index
2.10
2.08
2.06
2.04
2.02
2.00
10
20
30
40
PbO (mol%)

**Fig. 5.**

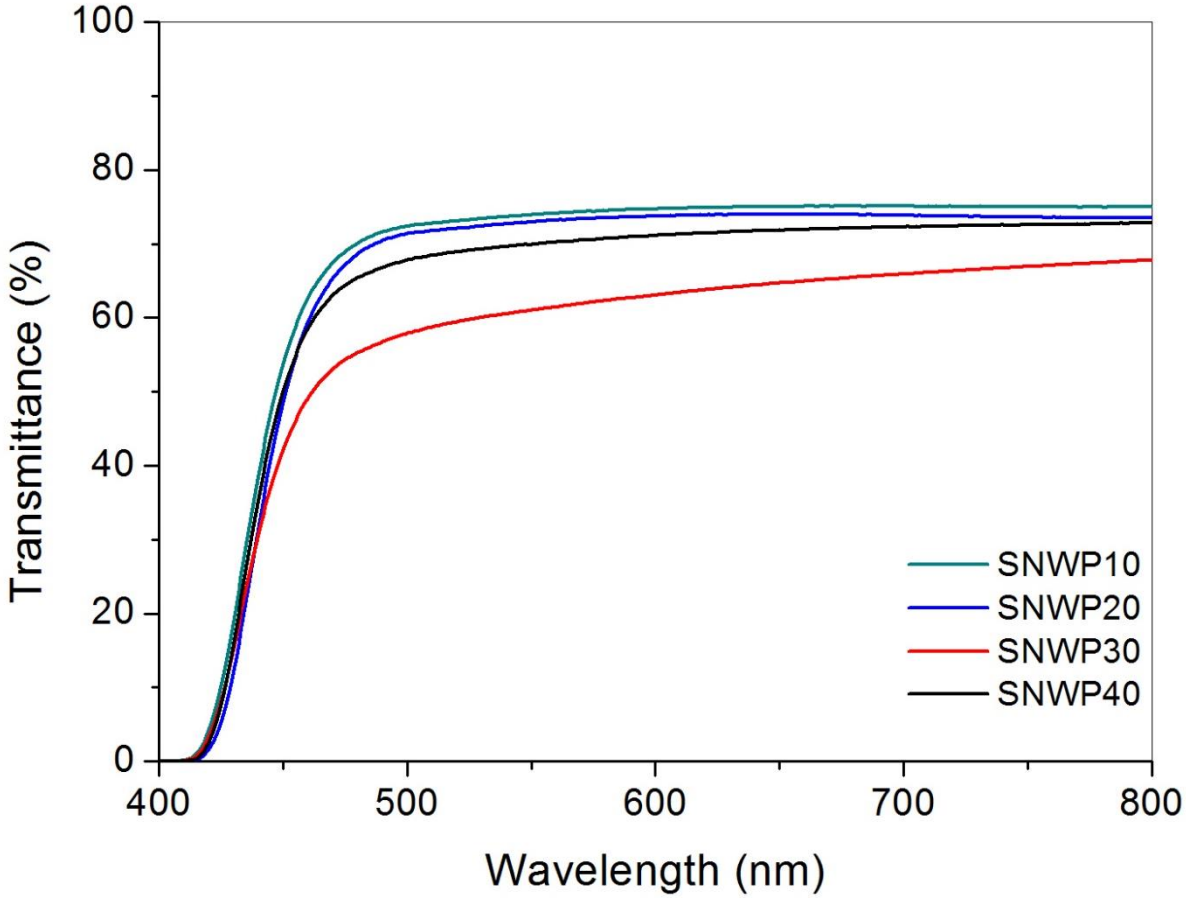
Transmittance (%)
Wavelength (nm)
SNWP10
SNWP20
SNWP30
SNWP40
0
20
40
60
80
100
400
500
600
700
800

**Fig. 6.**

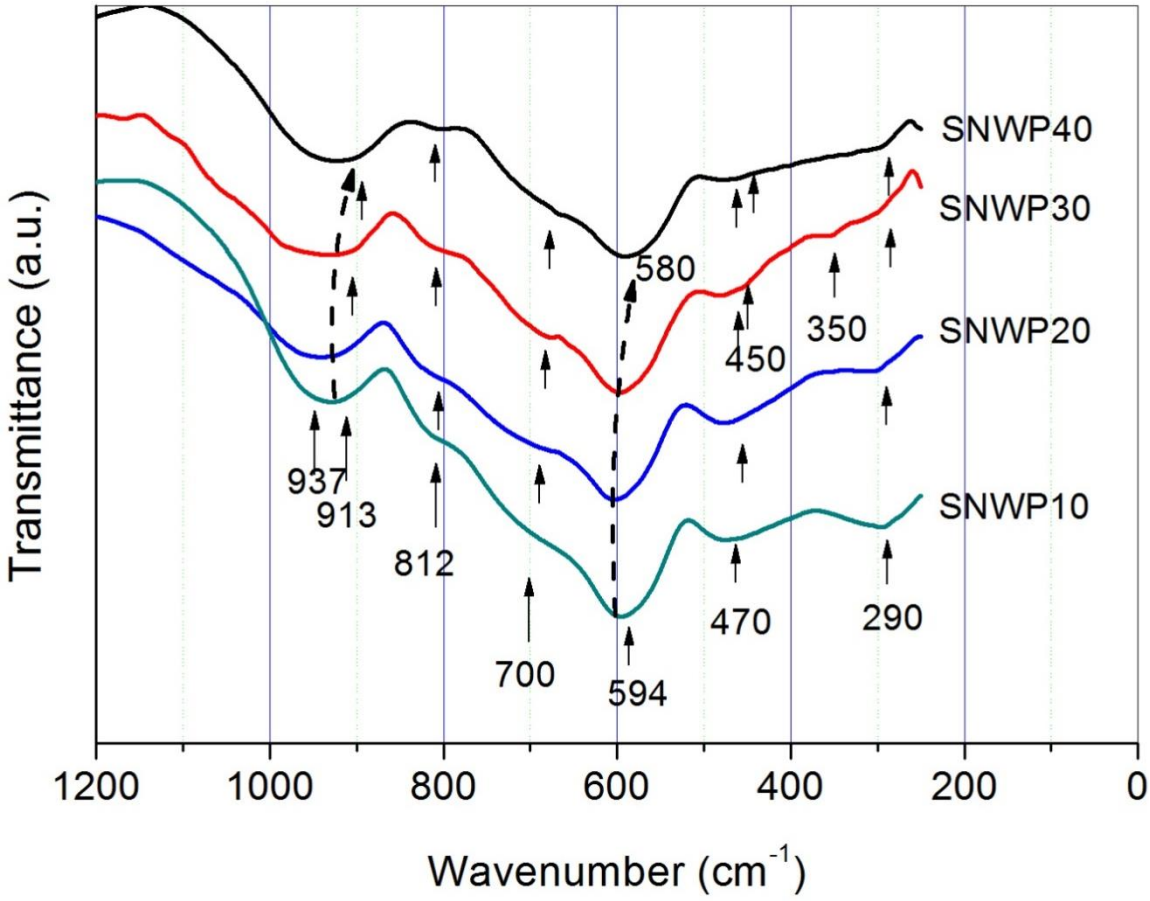
Transmittance (a.u.)
Wavenumber (cm-1)
SNWP40
SNWP30
SNWP20
SNWP10
580
450
350
937
913
812
700
594
470
290
1200
1000
800
600
400
200
0

**Fig. 7.**

# TABLES

**Table 1**

Values of glass transition ($T_g$) and first crystallization onset and peak ($T_{c1}/T_{p1}$) temperatures, glass stability ($\Delta T$), glass transition activation energy ($E_g$), fragility parameter ($m$), density ($\rho$), molar volume ($V_M$), oxygen molar volume ($V_O$), oxygen packing density (OPD), average cross-link density ($\overline{n_c}$), number of bonds per unit volume ($n_b$) and Poisson's ratio ($\mu_{cal}$) of $Sb_2O_3$-$Na_2O$-$WO_3$-PbO glasses.

| Sample ID | $Sb_2O_3$ | $Na_2O$ | $WO_3$ | PbO | $T_g$ (°C) | $T_{c1}$ / $T_{p1}$ (°C) | $\Delta T$ (°C) | $E_g$ (kj/mol) | $m$ | $\rho$ 25 °C ($g/cm^3$) | $\rho$ theoretical ($g/cm^3$) | $V_M$ ($cm^3$/mol) | $V_O$ ($cm^3$/mol) | OPD (mol/l) | $\overline{n_c}$ | $n_b$ ($x10^{21}$ $cm^{-3}$) | $\mu_{cal}$ |
|---|---|---|---|---|---|---|---|---|---|---|---|---|---|---|---|---|---|
| | mol% | | | | | | | | | | | | | | | | |
| SNWP10 | 68.57 | 10 | 11.43 | 10 | 287 | 373 / 408 | 86 | 330 | 70 | 5.31 | 5.56 | 48.01 | 31.55 | 54.16 | 2.21 | 75.24 | 0.174 |
| SNWP20 | 60 | 10 | 10 | 20 | 288 | 403 / 435 | 115 | 362 | 77 | 5.41 | 5.97 | 46.01 | 31.73 | 52.16 | 2.18 | 75.88 | 0.168 |
| SNWP30 | 51.43 | 10 | 8.57 | 30 | 289 | 362 / 413 | 73 | 377 | 80 | 5.53 | 6.37 | 43.93 | 31.87 | 50.08 | 2.16 | 76.73 | 0.163 |
| SNWP40 | 42.86 | 10 | 7.14 | 40 | 289 | 378 / 418 | 89 | 412 | 87 | 5.68 | 6.78 | 41.72 | 31.92 | 47.94 | 2.13 | 77.92 | 0.158 |

- : undetermined values

**Table 2**
Comparison of nominal and analyzed compositions of $Sb_2O_3$-$Na_2O$-$WO_3$-PbO glasses.

| Glasses | Theoretical (cat %) | | | | Analyzed (cat %) | | | | |
|---|---|---|---|---|---|---|---|---|---|
| | **Sb** | **Na** | **W** | **Pb** | **Sb** | **Na** | **W** | **Pb** | **Si** |
| SNWP10 | 76.80 | 11.20 | 6.40 | 5.60 | 77.92 | 8.63 | 7.54 | 5.82 | 0.09 |
| SNWP20 | 70.59 | 11.76 | 5.88 | 11.77 | 70.13 | 10.28 | 6.59 | 11.63 | 1.37 |
| SNWP30 | 63.72 | 12.39 | 5.31 | 18.58 | 62.25 | 11.03 | 5.85 | 18.36 | 2.51 |
| SNWP40 | 56.08 | 13.08 | 4.67 | 26.17 | 55.63 | 11.93 | 5.17 | 24.05 | 3.22 |

**Table 3**
Refractive indices and band gap of $Sb_2O_3$-$Na_2O$-$WO_3$-PbO glasses.

| Sample ID | Refractive index (±1.10$^{-4}$) at | | | | $E_g$ |
|---|---|---|---|---|---|
| | 632.8 nm | 825 nm | 1060.7 nm | 1551 nm | (eV) |
| SNWP10 | 2.0353 | 2.0180 | 2.0091 | 2.0033 | 2.979 |
| SNWP20 | 2.0799 | 2.0470 | 2.0310 | 2.0149 | 2.972 |
| SNWP30 | 2.0894 | 2.0560 | 2.0382 | 2.0221 | 2.975 |
| SNWP40 | 2.0953 | 2.0621 | 2.0431 | 2.0285 | 2.976 |